Flat Chern Band in a Two-Dimensional Organometallic Framework

Zheng Liu,[1] Zheng-Fei Wang,[1] Jia-Wei Mei,[2] Yong-Shi Wu,[3,4] and Feng Liu[1,*]

[1]*Department of Materials Science and Engineering, University of Utah, Salt Lake City, Utah 84112, USA*
[2]*Institute for Theoretical Physics, ETH Zurich, 8093 Zurich, Switzerland*
[3]*State Key Laboratory of Surface Physics and Department of Physics, Fudan University, Shanghai 200443, China*
[4]*Department of Physics and Astronomy, University of Utah, Salt Lake City, Utah 84112, USA*
(Received 29 October 2012; published 8 March 2013)

By combining exotic band dispersion with nontrivial band topology, an interesting type of band structure, namely, the flat Chern band, has recently been proposed to spawn high-temperature fractional quantum Hall states. Despite the proposal of several theoretical lattice models, however, it remains doubtful whether such a ''romance of flatland'' could exist in a real material. Here, we present a first-principles design of a two-dimensional indium-phenylene organometallic framework that realizes a nearly flat Chern band right around the Fermi level by combining lattice geometry, spin-orbit coupling, and ferromagnetism. An effective four-band model is constructed to reproduce the first-principles results. Our design, in addition, provides a general strategy to synthesize topologically nontrivial materials by virtue of organic chemistry and nanotechnology.

Whenever an unconventional band structure is brought out from a conceptual model into a real-world material, a wide range of theoretical advances and technological innovations will be triggered. The well-known examples are graphene [1,2] and topological insulators [3,4], which are featured with exotic dispersive bands and nontrivial topological bands, respectively. By combining these two features, another interesting type of band, namely, the flat Chern band (FCB), has recently been proposed [5–7], which is dispersionless and characterized by a nonzero Chern number. A well-defined FCB requires its bandwidth to be smaller than both the energy gap between the FCB and other bands and the interaction energy scale [5–7]. Since the kinetic energy is strongly quenched, carriers in the FCB experience strong Coulomb interaction in addition to the topological frustration that together spawn unprecedented topological strongly correlated electronic states [8–10]. Fundamentally different from the narrow bands commonly existing in heavy fermion compounds, which have a trivial Chern number, the outcome of a FCB requires a delicate balance of lattice hopping, spin-orbit coupling (SOC), and ferromagnetism. Because of the stringent criteria, no real material to date has been experimentally observed to contain a FCB.

Advances on synthetic chemistry and nanotechnology have shown the potential in producing complex lattices [11,12]. Recent experiments using substrate-mediated self-assembly have successfully fabricated 2D organometallic frameworks with different lattice symmetry. For example, Shi *et al.* [13] have synthesized two 2D frameworks by codepositing tripyridyl molecules with Fe and Cu atoms on the Au(111) surface, which form kagome and triangular lattices, respectively. These covalent organic frameworks are found to exhibit remarkable thermal stability. In this Letter, we present a first-principles design to realize the FCB in a 2D indium-phenylene organometallic framework (IPOF). Density functional theory (DFT) calculations [14] show that, in this unique IPOF structure, a nearly flat band appears around the Fermi level characterized by a nontrivial Z_2 topological number. Upon p-type doping, the spin degeneracy of the flat band is spontaneously lifted; the ferromagnetic flat band is then found to have a nontrivial Chern number.

Figure 1(a) shows the atomic structure of the IPOF, whose key feature is to bind p-orbital heavy elements (In) with organic ligands (paraphenylenes) into a hexagonal lattice. Each hexagonal unit cell contains three phenylenes and two In atoms. As a common feature of group-III elements, the In atoms naturally bond to three phenylenes in a planar triangular geometry. Such a bond configuration is identical to that in triphenyl-indium $In(C_6H_5)_3$, a common indium compound [15,16]. A similar organic framework assembled from 1,4-benzenediboronic acid on the Ag(111) surface has been fabricated in experiment, with only In atoms replaced by boroxine rings [17,18]. The stability of the IPOF has been examined by first-principles lattice relaxation and phonon calculations; details are discussed in Sec. II of the Supplemental Material [14]. The proposed synthesis process of the IPOF is described in Sec. III of the Supplemental Material [14].

To examine the electronic structure of the IPOF, we first purposely exclude SOC from the calculation. The resulting electronic band structure, wave function, and atomic-orbital projected density of states (DOS) are summarized in Fig. 1(c). The band structure presents a nonmagnetic insulator picture. Electronic bands at the band edge exclusively come from the p orbitals of C and In atoms. Specifically, at the valence edge, there are ten bands within
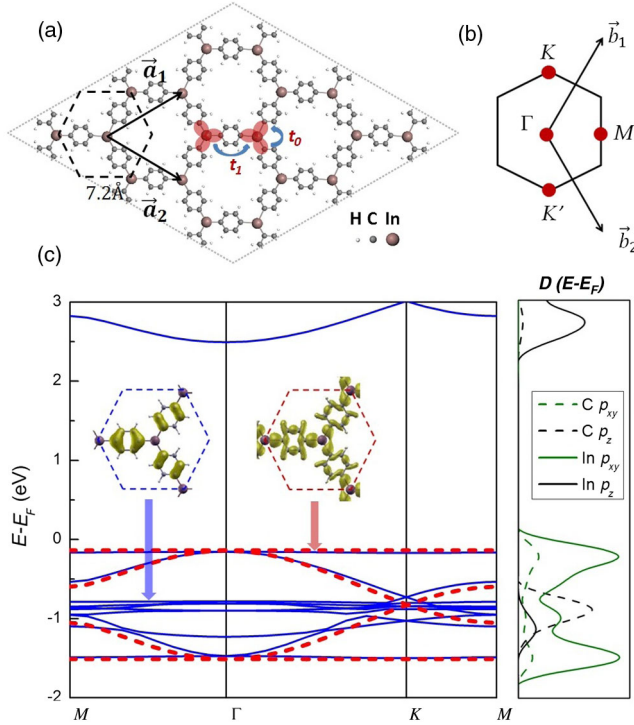
FIG. 1 (color online). (a) The atomic structure of the IPOF. (b) The first Brillouin zone and special k points. (c) (Left) Band structure without SOC from DFT [solid (blue) curves] and the model Hamiltonian Eq. (8) with $t_1 = 0.7$ eV, $\lambda = 0$, $M = 0$ [dashed (red) curves]. The insets are the wave function isosurfaces of the two states denoted by arrows. (Right) Atomic-orbital projected density of states.

FIG. 2 (color online). (a) Band structure with SOC. (b) Band structure with SOC when doping one hole into the unit cell. The solid (blue) curves are DFT results. The dashed (red) curves are from model Hamiltonian Eq. (8) with parameters (a) $t_1 = 0.7$ eV, $\lambda = 0.05$ eV, $M = 0$; (b) $t_1 = 0.7$ eV, $\lambda = 0.05$ eV, $M = 0.1$ eV. (c) Zoomed-in band plot around the Fermi level. (d) Momentum-resolved edge density of states of a semi-infinite IPOF with SOC and doping. The brightness is proportional to the magnitude of the density of states. (e) Distribution of the Berry curvature $F_{12}(\mathbf{k})$ of the top flat band in the reciprocal space. On the left is the DFT result; on the right is the model result using the same parameters as in (b).

2 eV from the valence band maximum, which can be divided into two groups. Around $E - E_F = 1$ eV, there are six p_z bands, which can be attributed to the highest π-electron molecular levels from the three benzene rings, as shown by both the wave function and the DOS. The remaining four bands exhibit in-plane p_{xy} features, which arise from hopping among the σ bonds between the In and C atoms [shaded (red) ellipses in Fig. 1(a)]. The top and bottom bands in the four p_{xy} bands are nearly flat in the whole Brillouin zone with a narrow bandwidth of 10 meV (without SOC). The middle two dispersive bands form a Dirac cone at the K points similar to graphene. The flat bands touch the dispersive bands at the Γ point. In contrast to the benzene molecular levels, the wave function of the p_{xy} flat bands surprisingly has a distribution across the whole lattice; i.e., they are not localized states [insets of Fig. 1(c)]. This is the first indication that these flat bands are unique and nontrivial.

Next, we include SOC in the calculation, and the results are shown in Fig. 2(a). Comparing Fig. 2(a) with Fig. 1(c), the most significant difference is that several degenerate points of the p_{xy} bands, e.g., the Γ and K points, are split. Consequently, the two flat bands become separated from the dispersive bands. The direct ($\Delta_{\mathrm{dir}}^{12}$) and indirect ($\Delta_{\mathrm{ind}}^{12}$)

gaps between the top flat band and the nearest dispersive band [Fig. 2(c)] are $\Delta_{\mathrm{dir}}^{12} = 90$ meV and $\Delta_{\mathrm{ind}}^{12} = 30$ meV. The separation between the top and bottom flat bands [Δ^{14} in Fig. 2(a)] is 1.4 eV. Another effect of the SOC splitting is that the band width (W) of the flat bands increases from 10 to 60 meV. Note that all the bands are still spin degenerate because of the time-reversal and inversion symmetry. The topology of the flat band is characterized by a nontrivial Z_2 topological number [3,4] as discussed in Sec. IV of the Supplemental Material [14].

The partially filled flat band is unstable due to the large DOS at the Fermi level. It has been rigorously proved that

even an arbitrarily small Coulomb interaction will drive the system into a ferromagnetic ground state at specific filling factors [19,20]. To obtain some insights within the DFT formalism, we dope the system by manually reducing the number of valence electrons in the unit cell, while maintaining the charge neutrality with a compensating homogeneous background charge. This makes the top flat band partially filled. Calculations reveal a spontaneous spin polarization perpendicular to the 2D plane. Figures 2(b) and 2(c) show the band structure of this ferromagnetic ground state under doping. The spin-up and spin-down bands are separated apart, with the Fermi level shifting below the topmost spin-polarized flat band. This ferromagnetic ground state is 5 meV lower than the spin-unpolarized state in total energy, which can be further stabilized by applying an external Zeeman field. The spin splitting $U \sim 100$ meV [Fig. 2(b)] represents the strength of the on-site Coulomb interaction. We thus estimate the electron-electron interaction of the p_{xy} electrons in the IPOF to be on the same order. For comparison, the spin splitting of the p_z electrons (benzene molecular levels) is 1 order of magnitude smaller.

We will now examine the topology of the topmost spin-polarized flat band by directly calculating its Chern number based on its DFT wave functions. The Chern number is defined as

$$c = \frac{1}{2\pi i} \int_{\text{BZ}} d^2\mathbf{k} F_{12}(\mathbf{k}), \tag{1}$$

where the Berry curvature $F_{12}(\mathbf{k})$ is given by

$$F_{12} = \partial_1 A_2(\mathbf{k}) - \partial_2 A_1(\mathbf{k}), \qquad A_i = \langle u_\mathbf{k} | \partial_i | u_\mathbf{k} \rangle. \tag{2}$$

$|u_\mathbf{k}\rangle$ is the Bloch function of the flat band, and the derivative ∂_i stands for $\partial / \partial_{k_i}$. The distribution of Berry curvature is shown in Fig. 2(e), exhibiting an interesting ring pattern. The integration of the Berry curvature in the whole Brillouin zone gives $c = 1$. Therefore, we conclude that this top flat band is a FCB.

A direct manifestation of the Chern number is the number of chiral edge modes circulating around the boundary. To check the edge property, we have calculated the momentum-resolved edge DOS of a semi-infinite IPOF [14]. As shown in Fig. 2(d), one single edge band emerges in the gap (Δ^{12}) and unidirectionally connects the top flat band with the dispersive band below it, signifying the typical feature of a chiral mode and indicating the Chern number $c = 1$.

The nonzero Chern number and chiral edge mode also suggest the existence of the quantum anomalous Hall effect in the IPOF, which has recently been predicted in graphene [21], magnetic topological insulator [22,23], and cold atoms [24,25]. In the prototyping quantum anomalous Hall model proposed by Haldane [26], the Berry curvature mainly distributes around the Brillouin zone corners due to the SOC-induced gap opening of the Dirac points.

For the IPOF, we have noticed that the Berry curvature mainly distributes around the Brillouin zone center, which is intuitively associated with the SOC-induced gap opening of the degenerate point (Γ point) between the flat band and the dispersive band. To further understand the origin of the FCB, we have constructed an effective Hamiltonian. Considering that the flat band comes from hopping among the σ bonds, we use these σ-bond orbitals as a basis to construct the effective Hamiltonian. There are three σ bonds around each In atom as marked by the shaded red ellipses in Fig. 1(a). We first symmetrize the basis orbitals by considering the nearest-neighbor (NN) hopping (t_0) among the three bonds:

$$H_0 = t_0 \begin{pmatrix} 0 & 1 & 1 \\ 1 & 0 & 1 \\ 1 & 1 & 0 \end{pmatrix}. \tag{3}$$

The eigenstates of H_0 consist of a doublet (ϵ_d) and a singlet (ϵ_s):

$$\epsilon_d = t_0, \qquad \Psi_{d1} = \frac{1}{\sqrt{2}}[1, 0, -1]^T, \qquad \Psi_{d2} = \frac{1}{\sqrt{6}}[1, -2, 1]^T;$$

$$\epsilon_s = -2t_0, \qquad \Psi_s = \frac{1}{\sqrt{3}}[1, 1, 1]^T. \tag{4}$$

The symmetrized eigenstates transform like vectors: Ψ_{d1} and Ψ_{d2} within the x-y plane and Ψ_s perpendicular to the x-y plane. As long as Ψ_s is far away from the doublet, it can be reasonably neglected. The problem is then reduced to a four-dimensional subspace spanned by two sets of Ψ_{d1} and Ψ_{d2} associated with the two In atoms in the unit cell. Considering the next-NN (NNN) hopping (t_1) via the benzene rings, we can write out a four-band hopping Hamiltonian for each spin:

$$H_{\text{hop}} = -t_1 \begin{pmatrix} 0 & 0 & V_{xx} & V_{xy} \\ 0 & 0 & V_{xy} & V_{yy} \\ V_{xx}^* & V_{xy}^* & 0 & 0 \\ V_{xy}^* & V_{yy}^* & 0 & 0 \end{pmatrix}, \tag{5}$$

in which $V_{xx} = \frac{1}{2}(1 + e^{i\mathbf{k}\cdot\mathbf{a}_1})$, $V_{xy} = \frac{\sqrt{3}}{2}(1 - e^{i\mathbf{k}\cdot\mathbf{a}_1})$, and $V_{yy} = \frac{1}{6}(1 + e^{i\mathbf{k}\cdot\mathbf{a}_1} + 4e^{i\mathbf{k}\cdot\mathbf{a}_2})$; $\mathbf{a}_{1,2}$ is the lattice vector as shown in Fig. 1(a). Without loss of generality, we have set the on-site energy of Ψ_{d1} and Ψ_{d2} as zero. The eigenvalues of H_{hop} give four energy bands [the dashed (red) curves in Fig. 1(c)], which agree well with the DFT results. H_{hop} effectively describes a honeycomb lattice with two in-plane vectorlike orbitals at each site, i.e., the p_{xy}-orbital counterpart of graphene. As discussed in Refs. [27,28], this kind of hopping Hamiltonian guarantees two completely flat bands because their Wannier functions forbid any electron ''leakage'' to the outside through a destructive interference.

With regard to SOC, we start from the original atomic form: $H_{SOC} = \lambda \hat{L} \cdot \hat{\sigma}$. By realizing that $\Psi_{d1,d2,s}$ transforms like three vectors, we can write out its second quantization form:

$$H_{SOC} = \lambda(ic_{d1\downarrow}^{\dagger}c_{d2\downarrow} - ic_{d1\uparrow}^{\dagger}c_{d2\uparrow} + c_{s\uparrow}^{\dagger}c_{d1\downarrow} - c_{s\downarrow}^{\dagger}c_{d1\uparrow}$$
$$+ ic_{s\uparrow}^{\dagger}c_{d2\downarrow} - ic_{s\downarrow}^{\dagger}c_{d2\uparrow} + \text{H.c.}), \quad (6)$$

in which $c_{i\sigma_z}^{\dagger}$ creates an electron with spin σ_z on the Ψ_i orbital. To reduce H_{SOC} into the four-band ($\Psi_{d1,d2}$) subspace, we keep only the leading terms:

$$H_{SOC}^0 = \lambda(ic_{d1\downarrow}^{\dagger}c_{d2\downarrow} - ic_{d1\uparrow}^{\dagger}c_{d2\uparrow}), \quad (7)$$

which do not include coupling between different spin components, so the spin-up and spin-down spaces get automatically separated. For each spin subspace, the SOC can also be written as a 4×4 matrix:

$$H_{SOC,\sigma_z}^0 = \sigma_z \lambda \begin{pmatrix} 0 & -i & 0 & 0 \\ i & 0 & 0 & 0 \\ 0 & 0 & 0 & -i \\ 0 & 0 & i & 0 \end{pmatrix}, \quad (8)$$

where $\sigma_z = \pm 1$ is the spin eigenvalue. This SOC represents an imaginary on-site coupling, independent of momentum. It pins an additional phase to the electrons when they hop between the two on-site orbitals and result in nontrivial topology when electrons travel in the lattice via H_{hop}.

The spontaneous magnetization under doping is a many-body effect [19,20]. Within the single-electron picture, we reproduce the ferromagnetism by simply adding a Zeeman term. Finally, the effective Hamiltonian to describe the single-electron property of the IPOF can be written as

$$H_{eff,\sigma_z = \pm 1}(k) = H_{hop}(k) + H_{SOC,\sigma_z}^0 + H_{Zeeman}$$
$$= -t_1 \begin{pmatrix} 0 & 0 & V_{xx} & V_{xy} \\ 0 & 0 & V_{xy} & V_{yy} \\ V_{xx}^* & V_{xy}^* & 0 & 0 \\ V_{xy}^* & V_{yy}^* & 0 & 0 \end{pmatrix}$$
$$+ \sigma_z \lambda \begin{pmatrix} 0 & -i & 0 & 0 \\ i & 0 & 0 & 0 \\ 0 & 0 & 0 & -i \\ 0 & 0 & i & 0 \end{pmatrix} + \sigma_z M. \quad (9)$$

There are three parameters in the model: The NNN hopping parameter t_1, the spin-orbit coupling strength λ, and the spontaneous magnetization M. Note that the NN hopping term t_0 does not explicitly enter the four-band model that renders the flat band more accessible in the IPOF than in other model lattices [5–7]. The higher-order hopping terms, e.g., the next-NNN hopping, will affect the

TABLE I. Energy scales associated with the FCB in the IPOF.

Property	Symbol	Value	Reference
Bandwidth	W	60 meV	Figure 2(c)
Spin splitting	U	100 meV	Figure 2(b)
Debye temperature	ω_d	300 meV	Figure S1 [14]
Energy gap	Δ_{dir}^{12}	90 meV	Figure 2(c)
	Δ_{ind}^{12}	30 meV	Figure 2(c)
	Δ^{14}	1.4 eV	Figure 2(a)

flatness, but they are already negligible in the IPOF, smaller than 10 meV, according to the DFT results. By fitting the three parameters to the DFT results, the dispersion of the four p_{xy} bands can be well reproduced, as is shown in Figs. 1(c), 2(a), and 2(b). To ensure that this simple model also reproduces the wave function property, we in addition calculate the Berry curvature using the model eigenstates; the result is also in good agreement with the DFT result [Fig. 2(e)]. The middle two dispersive bands from the model are found to have $c = 0$, as shown by the Berry curvature plot discussed in Sec. V of the Supplemental Material [14]; the bottom flat band has $c = -1$; thus, the total Chern number of the four-band subspace is zero. These justifications confirm the validity of the effective Hamiltonian, which will be useful for future investigations going beyond the DFT formalism.

In summary, we reiterate in Table I several key energy scales associated with the FCB in the IPOF. Further studies including many-body effects are necessary to determine the ground state and low-energy excitation of the carriers in the FCB. The emergence of the fractional quantum Hall state requires further enlarging the energy gap Δ^{12} and reducing the bandwidth W to satisfy the condition $\Delta \gg U > W$ [5,7,8]. To achieve this intriguing state, the organic nature of the IPOF provides the flexibility to tune the parameters in kinds of chemical ways, e.g., by functionalizing the benzenes with different chemical groups, replacing the benzenes with other organic ligands, or using different metal atoms. Furthermore, similar design principles can also be applied to realize other exotic band structures. For example, by simply replacing In with Bi and Mn, one makes a new organic topological insulator [29] and a new magnetic topological insulator [23], respectively.

official policies, either expressed or implied, of the ARL or the U.S. Government. The U.S. Government is authorized to reproduce and distribute reprints for Government purposes notwithstanding any copyright notation herein.

_____

*fliu@eng.utah.edu

[1] A. K. Geim, Rev. Mod. Phys. **83,** 851 (2011).
[2] K. S. Novoselov, Rev. Mod. Phys. **83,** 837 (2011).
[3] M. Z. Hasan and C. L. Kane, Rev. Mod. Phys. **82,** 3045 (2010).
[4] X.-L. Qi and S.-C. Zhang, Rev. Mod. Phys. **83,** 1057 (2011).
[5] T. Neupert, L. Santos, C. Chamon, and C. Mudry, Phys. Rev. Lett. **106,** 236804 (2011).
[6] K. Sun, Z. Gu, H. Katsura, and S. Das Sarma, Phys. Rev. Lett. **106,** 236803 (2011).
[7] E. Tang, J.-W. Mei, and X.-G. Wen, Phys. Rev. Lett. **106,** 236802 (2011).
[8] D. N. Sheng, Z.-C. Gu, K. Sun, and L. Sheng, Nat. Commun. **2,** 389 (2011).
[9] J. W. F. Venderbos, M. Daghofer, and J. van den Brink, Phys. Rev. Lett. **107,** 116401 (2011).
[10] Y.-F. Wang, Z.-C. Gu, C.-D. Gong, and D. N. Sheng, Phys. Rev. Lett. **107,** 146803 (2011).
[11] J. Sakamoto, J. van Heijst, O. Lukin, and A. D. Schluter, Angew. Chem., Int. Ed. Engl. **48,** 1030 (2009).
[12] J. V. Barth, G. Costantini, and K. Kern, Nature (London) **437,** 671 (2005).
[13] Z. Shi, J. Liu, T. Lin, F. Xia, P. N. Liu, and N. Lin, J. Am. Chem. Soc. **133,** 6150 (2011).
[14] See Supplemental Material at http://link.aps.org/supplemental/10.1103/PhysRevLett.110.106804 for discussions on calculation methods, lattice properties, a proposed synthesis process, the Z_2 topology of the flat band, and the Berry curvature of dispersive bands.
[15] H. Gilman and R. G. Jones, J. Am. Chem. Soc. **62,** 2353 (1940).
[16] A. McKillop, J. D. Smith, and I. J. Worrall, *Organometallic Compounds of Aluminum, Gallium, Indium, and Thallium*, Chapman and Hall Chemistry Sourcebooks (Chapman and Hall, London, 1985).
[17] N. A. A. Zwaneveld, R. Pawlak, M. Abel, D. Catalin, D. Gigmes, D. Bertin, and L. Porte, J. Am. Chem. Soc. **130,** 6678 (2008).
[18] O. Ourdjini *et al.*, Phys. Rev. B **84,** 125421 (2011).
[19] A. Mielke, J. Phys. A **24,** L73 (1991).
[20] A. Mielke, J. Phys. A **24,** 3311 (1991).
[21] Z. Qiao, S. A. Yang, W. Feng, W.-K. Tse, J. Ding, Y. Yao, J. Wang, and Q. Niu, Phys. Rev. B **82,** 161414 (2010).
[22] R. Yu, W. Zhang, H.-J. Zhang, S.-C. Zhang, X. Dai, and Z. Fang, Science **329,** 61 (2010).
[23] Z. Wang, Z. Liu, and F. Liu, arXiv:1302.1088.
[24] X.-J. Liu, X. Liu, C. Wu, and J. Sinova, Phys. Rev. A **81,** 033622 (2010).
[25] Y. Zhang and C. Zhang, Phys. Rev. B **84,** 085123 (2011).
[26] F. D. M. Haldane, Phys. Rev. Lett. **61,** 2015 (1988).
[27] C. Wu, D. Bergman, L. Balents, and S. Das Sarma, Phys. Rev. Lett. **99,** 070401 (2007).
[28] C. Wu and S. Das Sarma, Phys. Rev. B **77,** 235107 (2008).
[29] Z. Wang, Z. Liu, and F. Liu, Nat. Commun. **4,** 1471 (2013).